Enhanced luminescence from GaN nanopillar arrays fabricated using top-down process

N Parvathala Reddy [†, a], Shagufta Naureen[†, b], Sudha Mokkapati[†], Kaushal Vora[‡], Naeem Shahid[‡], Fouad Karouta[‡], Hark Hoe Tan[†], and Chennupati Jagadish[†]

[†]Department of Electronic Materials Engineering, Research School of Physics and Engineering, The Australian National University, Canberra, ACT 2601, Australia

‡Australian National Fabrication Facility, Research School of Physics and Engineering, The Australian National University, Canberra, ACT 2601, Australia

Corresponding Author: [a] parvathala.narangari@anu.edu.au; [b] shagufta.naureen@anu.edu.au

Abstract

We report the fabrication of GaN nanopillar arrays with good structural uniformity using the top-down approach. The photoluminescence intensity from the nanopillar arrays is enhanced compared to the epilayer. We use FDTD simulations to show that the enhancement in photoluminescence intensity from the nanopillar arrays is a result of anti-reflection properties of the arrays that result in enhanced light absorption and increase in light extraction efficiency compared to the epilayer. The measured quantum efficiency of the nanopillars is comparable to that of epitaxially grown GaN epilayer.

Introduction

(Al, In)GaN material system has received a lot of interest since its commercialization for solid state lighting applications[1]. Direct band gap, tunable from 0.7 eV (for InN) to 6.2 eV (for AlN), makes this material system ideal for optoelectronic applications. Sapphire is the common substrate of choice for hetero-epitaxy of this material system. Lattice mismatch between the substrate and the epilayer introduces strain induced piezoelectric polarization, which limits the performance of devices fabricated in this material system [2].

Nanopillars or nanowires offer an alternative to mitigate the difficulties associated with planar structures in this material system. Nanopillar (NP) sidewalls can be used as non-polar or semi-polar facets for epitaxial growth to form core-shell device structures [3, 4] which increase the active junction area and mitigate polarization effects. Several optoelectronic devices based on GaN NPs such as LEDs [5-7], photodetectors [8-10] and solar cells [4, 11] have already been demonstrated. NPs can be fabricated using bottom-up growth [12-14] or top-down etch processes [15]. Lack of control over the doping profile, critical for device applications, is the major set-back for bottom-up approach [16, 17]. Top-down approach on the other hand is more suitable as it involves etching of epitaxial layers of high crystal quality grown using a well-established technique such as metal organic chemical vapor deposition (MOCVD) wherein doping and layer thickness are precisely controlled.

Dipak et. al. [15, 18] have reported a comprehensive study on the fabrication of GaN NPs and the influence of various etching parameters such as gas chemistry, ICP/RF power, chamber pressure and substrate temperature on the NP morphology. There are also some reports on enhancement in PL emission intensity from GaN NP arrays compared to that from an epilayer [19-21]. In this work, we study the influence of array pitch on morphology of GaN NPs and photoluminescence (PL) of NP arrays fabricated using inductively coupled plasma

reactive ion etching (ICP-RIE) of electron beam lithography (EBL) patterned epilayers. We explain the PL emission characteristics of GaN NP arrays using extensive FDTD simulations. We also quantify the quantum efficiency of the GaN NPs through power dependent PL measurements.

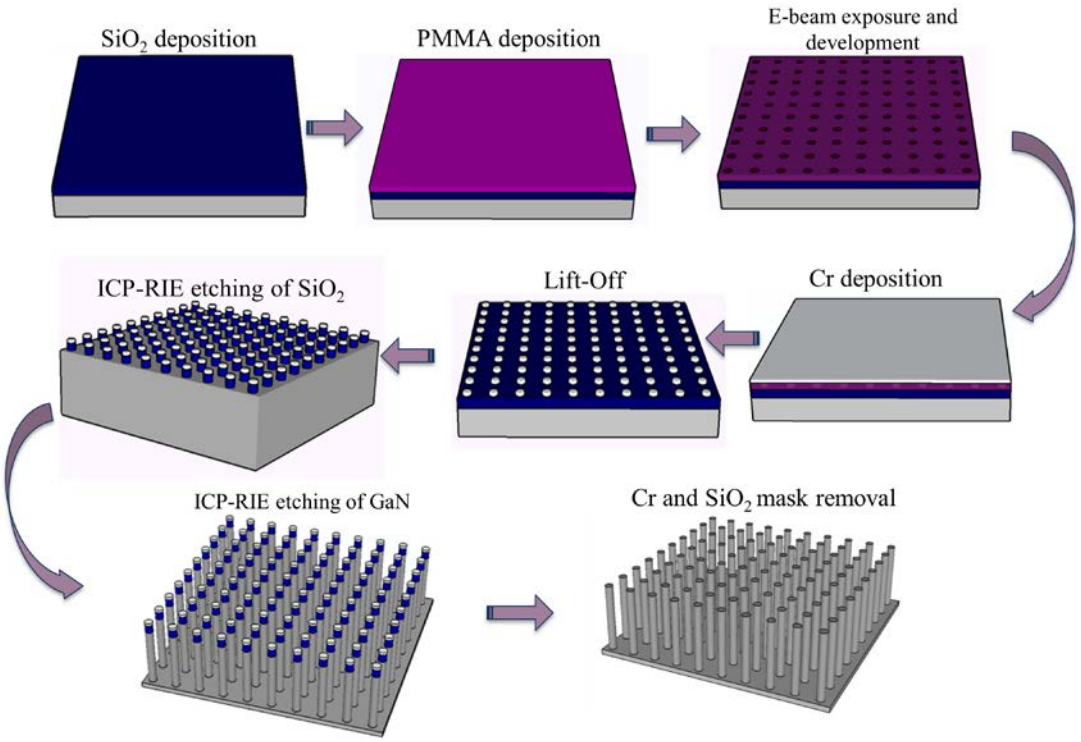

Figure 1: Flow chart of processing steps involved in top-down fabrication of GaN NPs.

Experimental

Figure 1 illustrates the process flow for the fabrication of GaN NPs using top-down method. Plasma enhanced chemical vapour deposition (Oxford Plasmalab 100) was used to deposit SiO_2 (500 nm) on 2 μm-thick epitaxial GaN layers grown by MOCVD on sapphire substrates. Next, an electron-beam sensitive PMMA resist was spin-coated onto these samples and patterned using EBL (Raith 150) to obtain an array of circular holes with a diameter of 100 nm and pitch ranging from 400 to 800 nm. After developing the exposed resist in MIBK, 100 nm Cr layer was deposited on the sample using electron beam evaporation (Temescal BJD-

2000). Following lift-off in acetone, the sample had arrays of Cr nano-disks patterned on its surface. These Cr nano-disks were used as a mask for etching the SiO_2 layer underneath by ICP-RIE (Versaline LL). ICP-RIE operating at 10 mT with a CHF_3 flow of 40 sccm is used to etch the SiO_2 layer at a substrate temperature of 20^{o}C. ICP and RF powers were 30 and 1000 W, respectively. The resulting stack of Cr/SiO_2 nano-disks was subsequently used as a mask for fabricating GaN NP of desired dimensions using ICP-RIE. For ICP-RIE of GaN, the flows of Cl_2, Ar and H_2 were 25, 5, and 2 sccm respectively with ICP/RF power of 1000/200 Watt, operating pressure of 4 mTorr and sample temperature at 60 ^{o}C. Cr etchant solution (Sigma Aldrich) and barrel etcher (PVA TePla) with O_2/CF_4 chemistry were then used to remove the Cr and SiO_2 mask, respectively. All the NP arrays studied here were fabricated simultaneously on the same wafer to avoid variations in etch conditions between different etch runs.

The NP arrays were structurally characterised using a scanning electron microscope (SEM) (FEI Helios 600 Nanolab). Optical/optoelectronic quality of the NPs was evaluated at room temperature using excitation power dependent PL measurements. The samples were optically excited with a continuous-wave 325 nm He-Cd laser and the emission from the samples was collected through a 36X (NA=0.5) objective lens and detected using a Si CCD. The optical properties of the NP arrays are explained using three dimensional finite difference time domain (FDTD) simulations [22].

Results and Discussion

Figure 2(a)-(c) shows SEM images of NP arrays with a pitch of 400, 600 and 800 nm, respectively. The NP arrays have smooth sidewalls and a constant height of 1.3 μm. Under the fabrication conditions used in this study, we did not observe any noticeable variation in the NP height due to lag effect [23]. We observed variation in tapering (sloped sidewalls) of the NPs with the pitch of the array as shown in SEM images (Figure 2(a)-(c)). Sloped sidewalls at higher

pitches indicate that etching of GaN is dominated by the physical etching component also called sputter dominated regime [23]. The trenching observed at the bottom of the NPs at higher pitch can be a result of angular distributed ions, collected at the bottom of NP upon colliding with a sidewall. The ions may have higher chances to colloid at a glancing angle before reaching at the bottom of NP when the sidewall is tapered. With lowering pitch, ions hitting under angle have higher chance of bouncing and hitting the surrounding NP sidewall before reaching the bottom of the surface and as such contribute to the near vertical shape of the NPs. This results in reduced tapering of NPs with reducing pitch.

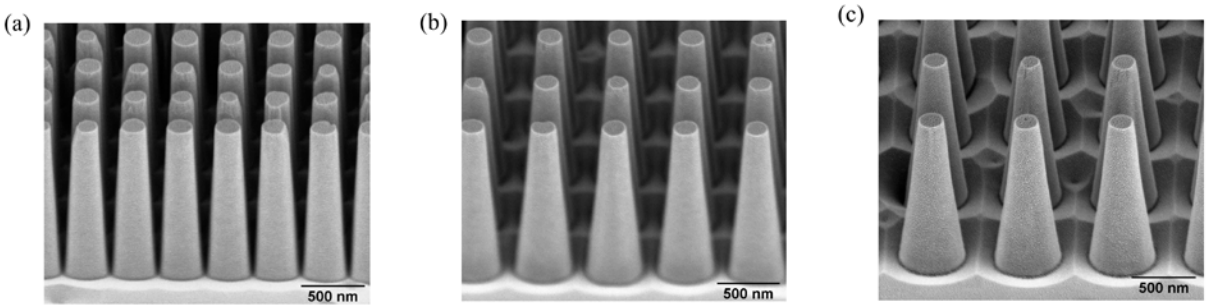

Figure 2: SEM images of GaN NP arrays pitch of (a) 400 nm (b) 600 nm and (c) 800 nm taken at 52º tilt angle.

We investigated the optical/optoelectronic quality of the NPs using μ-PL. Figure 3(a) shows the room-temperature PL spectra from the NP arrays and the epilayer. The emission peak in the spectra from the NP arrays is shifted towards lower energy (red shift) compared with the emission peak for the epilayer, and it is invariant with pitch. Partial strain relaxation of NPs might have caused red shift of the peak position [18]. The intensity of PL emission from the NP arrays is higher than that from an epilayer for all pitches investigated. There is no significant contribution from the ~700 nm-thick epilayer, left underneath the NP arrays after etching, to the PL emission from the arrays, as will be shown later in the manuscript. Peak emission from the array with 400 nm pitch is ~4 times more intense than that from an epilayer under the same experimental excitation and collection conditions. PL enhancement for NPs

makes them a promising candidate for solid state lighting applications. Emission intensity from the NP arrays reduces with increasing pitch. The variation in emission intensity for the NPs could be a result of variation in the quantum efficiency (QE) of the NPs or variation in light absorption [24] and collection efficiency. QE, defined as the ratio of radiative recombination rate to the total recombination rate, is an indication of the material quality of the sample while the absorption/collection efficiency is a geometrical property of the array.

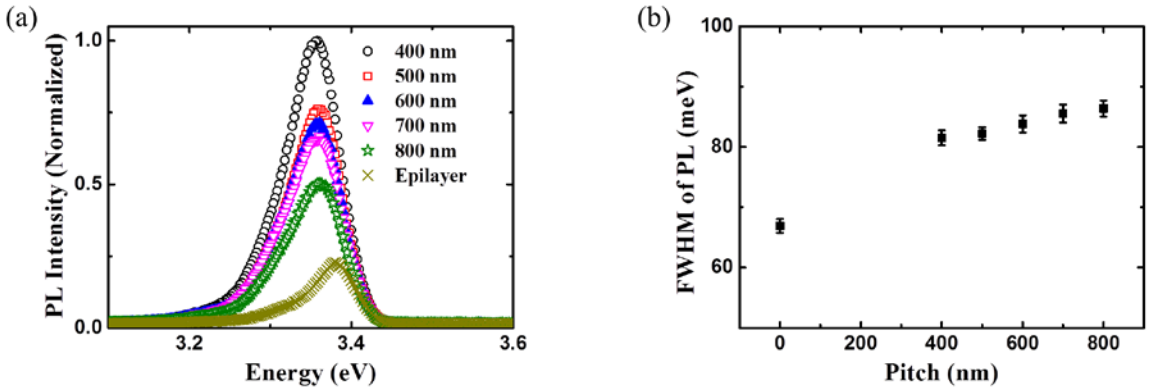

Figure 3: (a) Photoluminescence (PL) spectra from NP arrays of varying pitch and (b) full width at half maximum of the PL as a function of array pitch. Data for GaN epilayer is also shown for comparison at pitch=0.

The full width at half maximum (linewidth) of the PL spectra, determined by fitting the experimental data in Figure 3(a) with a Gaussian, is shown in Figure 3(b). The PL linewidth for the NPs is slightly larger compared to the epilayer. This broadening of PL emission could be due to ion damage caused to the NP sidewalls during ICP-RIE etching. Furthermore, there is a slight trend of increasing linewidth by increasing the pitch of NP arrays. As discussed earlier tapering increases with increasing pitch and this may contribute to an increase in FWHM of PL emission as a result of strain variation along the length of the NPs [18].

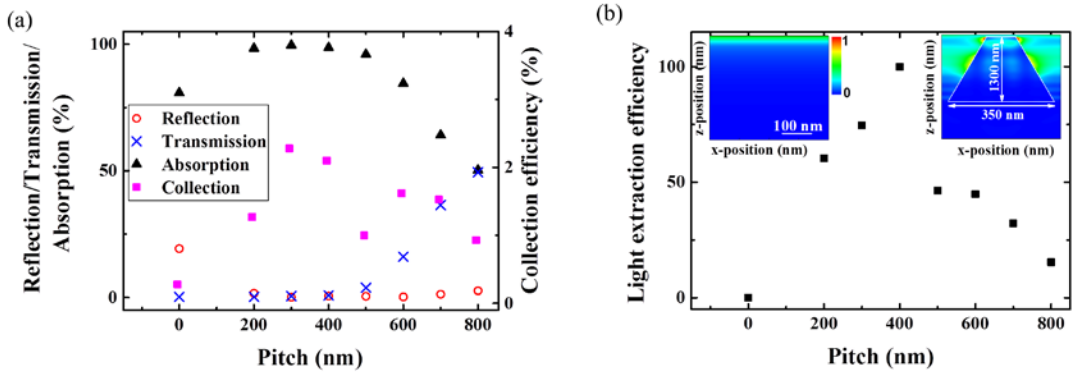

Figure 4: Influence of array pitch on (a) reflection, transmission, absorption and collection efficiency. The scale for reflection, transmission and absorption is shown on the left side and the scale for collection efficiency is shown on the right and (b) light extraction efficiency. Inset shows the electric field distribution of incident radiation in epilayer (left) and NP (right).

To explain the emission characteristics shown in Figure 3(a), we investigated the effect of array parameters on light absorption and emission characteristics using three dimensional FDTD simulations. NP arrays with infinite extension were simulated. Length, tapering and GaN epilayer leftover underneath the NP array were taken into consideration in simulations. To determine the absorption characteristics, the sample was illuminated by a plane wave source and the fraction of incident power reflected and transmitted through the sample was recorded at a wavelength of 325 nm. Absorption was determined by calculating the sum of reflection and transmission and subtracting it from incident power. Figure 4 (a) shows the variation in fraction of incident power reflected, transmitted and absorbed in the NP array as a function of pitch. The data for the epilayer (i.e. at pitch=0) is also included for comparison. The NP arrays have geometry dependent absorption characteristics that are very different to absorption in an epilayer. The absorption efficiency for the NP array with 400 nm pitch is 98.6%, which is 1.2 times larger than that of an epilayer (80.6%). The absorption efficiency reduces with increasing pitch and falls below that in an epilayer for pitch > 600 nm. This property is a consequence of

the change in both the reflection and transmission properties of the NP arrays. The reflection losses for the NP arrays is significantly reduced (~0.25%) compared to an epilayer (19.3%). For NP arrays with dimensions much less than the wavelength of light, anti- reflection characteristics can be attributed to lower effective index of the array compared to bulk material [25].Effective medium theory is however, not applicable to our NP arrays because of their wavelength-scale dimensions. We attribute lower reflection losses in our NP arrays to better in-coupling of incident light to the resonant modes supported in the array [25]. The transmission loss for the NP arrays is higher than in an epilayer because of reduced absorption volume. The transmission loss increases with increasing pitch and reaches 47% for a pitch of 800 nm. Therefore, we attribute the increase in absorption efficiency of NPs with 400 nm pitch to reduced reflection losses and subsequent lowering of absorption for larger pitches to increase in transmission losses. The inset in Figure 4(b) shows the electric field intensity distribution across the epilayer and a NP in an array of 400 nm pitch. The field distributions show that incident light is strongly absorbed within few 10s of nm from the top surface of the samples, eliminating any contribution from the GaN epilayer underneath the NP to PL when the arrays are characterized.

Apart from differences in light absorption, the emission characteristics of NP arrays are also very different to that of an epilayer. The parameters of the array alter the angular distribution of emission from NPs. The angular distribution of emission determines the fraction of light emitted by the sample that is detected in our experiments, which is limited by the numerical aperture of the objective lens used. We placed dipole emitters inside the NPs at regions of maximum absorption (insets of Figure 4(b)) and investigated their far-field emission characteristics. We then calculated the fraction of emitted light within a cone with a half angle of 30^{o}, corresponding to the numerical aperture of the objective lens used in our experiments. This data is represented as the collection efficiency in Figure 4(a) and is the average for three

different polarisations of the dipole emitters. We observe two peaks in the collection efficiency data at 300 and 600 nm pitches, which is due to the first and second diffraction orders falling just below the collection angle in our experimental setup, respectively.

The ordered structure of the NP arrays also modifies the local density of optical states for the emitters and therefore alters their recombination rates [26]. This would affect the emission intensity from the sample. We determined the recombination rate enhancement for dipole emitters placed at regions of maximum absorption, with respect to an emitter in bulk GaN, and studied the emission at 367 nm for epilayer and at 370 nm for NPs which correspond to the respective peak positions shown in Figure 3(a).

The PL emission intensity depends on the product of absorption and collection efficiencies and the emission rate enhancement, shown as light extraction efficiency in Figure 4(b). The light extraction efficiency follows the same trend observed in PL intensities (Figure 3(a)). Thus we believe that the change in PL emission intensities from the NP arrays is purely a geometrical effect.

We also experimentally determined QE of the GaN epilayer and the NPs using the approach outlined by Yang Seok Yoo et. al [27] in order to investigate the effect of the fabrication method on the material quality. The measured variation in PL intensity from the epilayer and the NP array (pitch 400 nm) with excitation power at room temperature, using a CW excitation at 325 nm is shown in Figure 5(a). The excitation power is varied between 0.06 and 1.2 mW. The excitation power range is limited by the minimum power at which we were able to detect PL emission and the maximum power emitted by the excitation laser. The emission intensity from the epilayer is lower than from the NP array for the range of excitation powers investigated.

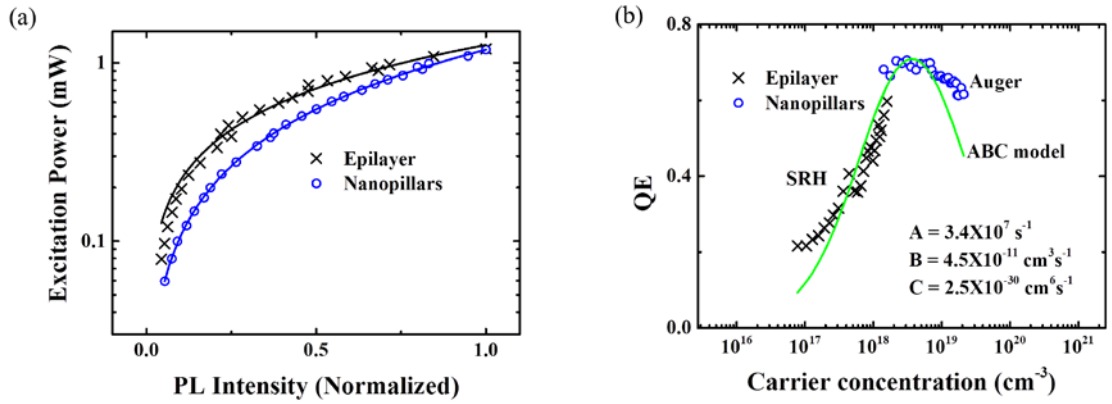

Figure 5: (a) Excitation power vs. PL intensity and (b) dependence of quantum efficiency (QE) on carrier concentration. The points are experimental data and the lines are fits to experimental data following the approach of Yang Seok Yoo et. al.[27].

Figure 5(b) shows the QE vs. carrier density data for the epilayer and the NP array. The photo-generated carrier density, n, in the epilayer and the NP array is calculated by $n = \frac{PA\tau}{E_g V}$, where P is power, A is absorption, τ is effective carrier life time, E_g is band gap energy and V is the volume over which the carriers are generated. Absorption data calculated using FDTD simulations as discussed earlier is used. The absorption depth (inset of Figure 4(b)) and the excitation laser spot size are used to calculate the volume, V. We use an effective carrier lifetime of 30 ps [28]. The maximum and minimum power of the excitation source used in our experimental set-up limits the carrier density range in epilayer and the NP array to the values shown in Figure 5(b). This limits us from determining the QE for the epilayer and the NP array at the same carrier density.

Figure 5(b) shows that QE of the epilayer increases with increasing carrier density reaching a value of 0.6 at a carrier density of 1.58×10^{18} cm^{-3}. Variation of QE with carrier density suggests that QE is limited by the Shockley-Read-Hall (SRH) recombination. With increasing carrier density, the radiative recombination rate increases and exceeds the monomolecular recombination rate leading to increase in QE. On the other hand, the variation

of QE of NPs with carrier density suggests that the carrier density in the NPs is in the region where Auger recombination becomes dominant and hence QE starts to decrease with increasing carrier concentration. The QE of the NPs is 0.71 at a carrier density of 3.11×10^{18} cm^{-3} and falls to 0.62 at a carrier density of 2.10×10^{19} cm^{-3}.

Figure 5(b) also shows the analytically calculated QE variation with injected carrier density using the 'ABC model' [27] assuming the coefficients are the same for epilayer and NPs, and do not vary with carrier density. The A, B and C coefficients determine the variation in monomolecular SRH recombination, radiative recombination and Auger recombination with carrier density respectively. The A, B and C coefficients used to obtain a good fit to data points across the entire carrier concentration range (i.e., using data points for the epilayer for lower carrier densities and data points for the NP array for higher carrier densities) are also indicated, and agree well with the values reported earlier [29-31]. The fact that a single analytical curve fits both datasets indicates reasonably well that the material quality of the NPs is not degraded due to the etching process, and both epilayer and NPs maintain similar optoelectronic quality.

Conclusions

We studied the optical/optoelectronic properties of GaN NP arrays fabricated by etching EBL patterned GaN epilayer using ICP-RIE. Despite lower semiconductor volume, the NP arrays exhibit stronger photoluminescence intensity compared to the epilayer. FDTD simulations confirm that this is a consequence of enhanced light absorption and light extraction efficiency in the NP arrays. We experimentally determined the quantum efficiency of the NPs, and found it to be similar to that of the epilayer, indicating that the material quality of the NPs is not degraded by the fabrication process.

Acknowledgements

We acknowledge the Australian Research Council (ARC), the Australian National Fabrication Facility (ANFF), A. C. T. node and the National Computational Infrastructure (NCI) for financial support, access to experimental facilities and computational resources, respectively.

References

[1] Nakamura S, Senoh M and Mukai T 1993 P-Gan/N-Ingan/N-Gan Double-Heterostructure Blue-Light-Emitting Diodes *Jpn J Appl Phys 2* **32** L8-L11

[2] Ryou J H, Yoder P D, Liu J P, Lochner Z, Kim H, Choi S, Kim H J and Dupuis R D 2009 Control of Quantum-Confined Stark Effect in InGaN-Based Quantum Wells *Ieee Journal of Selected Topics in Quantum Electronics* **15** 1080-91

[3] Chang J R, Chang S P, Li Y J, Cheng Y J, Sou K P, Huang J K, Kuo H C and Chang C Y 2012 Fabrication and luminescent properties of core-shell InGaN/GaN multiple quantum wells on GaN nanopillars *Applied Physics Letters* **100** 261103

[4] Wierer J J, Jr., Li Q, Koleske D D, Lee S R and Wang G T 2012 III-nitride core-shell nanowire arrayed solar cells *Nanotechnology* **23** 194007

[5] Wang C Y, Chen L Y, Chen C P, Cheng Y W, Ke M Y, Hsieh M Y, Wu H M, Peng L H and Huang J 2008 GaN nanorod light emitting diode arrays with a nearly constant electroluminescent peak wavelength *Opt Express* **16** 10549-56

[6] Ra Y H, Navamathavan R, Park J H and Lee C R 2013 Coaxial In(x)Ga(1-x)N/GaN multiple quantum well nanowire arrays on Si(111) substrate for high-performance light-emitting diodes *Nano letters* **13** 3506-16

[7] Wang G T, Li Q, Wierer J J, Koleske D D and Figiel J J 2014 Top-down fabrication and characterization of axial and radial III-nitride nanowire LEDs *physica status solidi (a)* **211** 748-51

[8] Bugallo Ade L, Tchernycheva M, Jacopin G, Rigutti L, Julien F H, Chou S T, Lin Y T, Tseng P H and Tu L W 2010 Visible-blind photodetector based on p-i-n junction GaN nanowire ensembles *Nanotechnology* **21** 315201

[9] Babichev A V, Zhang H, Lavenus P, Julien F H, Egorov A Y, Lin Y T, Tu L W and Tchernycheva M 2013 GaN nanowire ultraviolet photodetector with a graphene transparent contact *Applied Physics Letters* **103** 201103

[10] Wang X, Zhang Y, Chen X, He M, Liu C, Yin Y, Zou X and Li S 2014 Ultrafast, superhigh gain visible-blind UV detector and optical logic gates based on nonpolar a-axial GaN nanowire *Nanoscale* **6** 12009-17

[11] Dong Y, Tian B, Kempa T J and Lieber C M 2009 Coaxial group III-nitride nanowire photovoltaics *Nano letters* **9** 2183-7

[12] Hersee S D, Sun X Y and Wang X 2006 The controlled growth of GaN nanowires *Nano letters* **6** 1808-11

[13] Lin Y-T, Yeh T-W, Nakajima Y and Dapkus P D 2014 Catalyst-Free GaN Nanorods Synthesized by Selective Area Growth *Advanced Functional Materials* **24** 3162-71

[14] Qian F, Li Y, Gradecak S, Park H G, Dong Y, Ding Y, Wang Z L and Lieber C M 2008 Multi-quantum-well nanowire heterostructures for wavelength-controlled lasers *Nature materials* **7** 701-6

[15] Paramanik D, Motayed A, Aluri G S, Ha J-Y, Krylyuk S, Davydov A V, King M, McLaughlin S, Gupta S and Cramer H 2012 Formation of large-area GaN nanostructures with controlled geometry and morphology using top-down fabrication scheme *Journal of Vacuum Science & Technology B: Microelectronics and Nanometer Structures* **30** 052202

[16] Tessarek C, Heilmann M, Butzen E, Haab A, Hardtdegen H, Dieker C, Spiecker E and Christiansen S 2014 The Role of Si during the Growth of GaN Micro- and Nanorods *Crystal Growth & Design* **14** 1486-92

[17] Yang P, Yan R and Fardy M 2010 Semiconductor nanowire: what's next? *Nano letters* **10** 1529-36

[18] Debnath R, Ha J-Y, Wen B, Paramanik D, Motayed A, King M R and Davydov A V 2014 Top-down fabrication of large-area GaN micro- and nanopillars *Journal of Vacuum Science & Technology B: Microelectronics and Nanometer Structures* **32** 021204

[19] Ng W N, Leung C H, Lai P T and Choi H W 2008 Nanostructuring GaN using microsphere lithography *Journal of Vacuum Science & Technology B: Microelectronics and Nanometer Structures* **26** 76

[20] Zhu J, Wang L, Zhang S, Wang H, Zhao D, Zhu J, Liu Z, Jiang D and Yang H 2010 The fabrication of GaN-based nanopillar light-emitting diodes *Journal of Applied Physics* **108** 074302

[21] Li K H and Choi H W 2011 Air-spaced GaN nanopillar photonic band gap structures patterned by nanosphere lithography *Journal of Applied Physics* **109** 023107

[22] I L S http://www.lumerical.com/tcad-products/fdtd/.

[23] Rong B, Salemink H W M, Roeling E M, van der Heijden R, Karouta F and van der Drift E 2007 Fabrication of two dimensional GaN nanophotonic crystals (31) *Journal of Vacuum Science & Technology B: Microelectronics and Nanometer Structures* **25** 2632

[24] Zhu J, Yu Z, Burkhard G F, Hsu C M, Connor S T, Xu Y, Wang Q, McGehee M, Fan S and Cui Y 2009 Optical absorption enhancement in amorphous silicon nanowire and nanocone arrays *Nano letters* **9** 279-82

[25] Mokkapati S and Catchpole K R 2012 Nanophotonic light trapping in solar cells *Journal of Applied Physics* **112** 101101

[26] Purcell E M, Torrey H C and Pound R V 1946 Resonance Absorption by Nuclear Magnetic Moments in a Solid *Physical Review* **69** 37-8

[27] Yoo Y-S, Roh T-M, Na J-H, Son S J and Cho Y-H 2013 Simple analysis method for determining internal quantum efficiency and relative recombination ratios in light emitting diodes *Applied Physics Letters* **102** 211107

[28] Kwon H K, Eiting C J, Lambert D J H, Wong M M, Dupuis R D, Liliental-Weber Z and Benamara M 2000 Observation of long photoluminescence decay times for high-quality GaN grown by metalorganic chemical vapor deposition *Applied Physics Letters* **77** 2503

[29] Dmitrieva A and Oruzheinikov A 1999 The rate of radiative recombination in the nitride semiconductors and alloys *Journal of Applied Physics* **86** 6

[30] Bulashevich K A and Karpov S Y 2008 Is Auger recombination responsible for the efficiency rollover in III-nitride light-emitting diodes? *physica status solidi (c)* **5** 2066-9

[31] Kioupakis E, Rinke P, Delaney K T and Van de Walle C G 2011 Indirect Auger recombination as a cause of efficiency droop in nitride light-emitting diodes *Applied Physics Letters* **98** 161107